analytical chemistry

Article

pubs.acs.org/ac

Semiautomated Support Photoelectrochemical Immunosensing Platform for Portable and High-Throughput Immunoassay Based on Au Nanocrystal Decorated Specific Crystal Facets $BiVO_4$ Photoanode

Jian Shu, Zhenli Qiu, Zhenzhen Lin, Guoneng Cai, Huanghao Yang, and Dianping Tang*

Key Laboratory of Analysis and Detection for Food Safety (MOE and Fujian Province), Collaborative Innovation Center of Detection Technology for Haixi Food Safety and Products (Fujian Province), State Key Laboratory of Photocatalysis on Energy and Environment, Department of Chemistry, Fuzhou University, Fujian Province, China, 350002

Supporting Information

ABSTRACT: Photoelectrochemical (PEC) measurement has been developed rapidly for bioanalysis in recent years. However, the actual application for most existed PEC bioanalytical systems is still a challenge because the perfect solutions for sensing surface design, high-throughput detection, and portability are lacked. To successfully overcome these limitations and realize accurate, continuous screening and assessing on prognostic indicator of early stage cancer on the spot, an innovative and portable semiautomated support power-free photoelectrochemical (SP-PEC) immunosensing platform consisted with a miniature semiautomatic injection system and digital multimeter (DMM) readout is designed (prostate specific antigen, PSA, was used as the proof-of-concept analyte). Decahedral $BiVO_4$ that decorated with Au nanocrystal on {010} facets (Au-$BiVO_4$) by photodeposition is used as the photoanode materials to produce photocurrent signal under irradiation of micro laser light (5.0 w, $\lambda \geq 380$ nm). The monoclonal anti-PSA capture antibody (mAb_1)-functionalized Fe_3O_4 magnetic nanobeads (mAb_1-MN) and glucose oxidase (GOx)/monoclonal detection antibody (mAb_2)-conjugated gold nanoparticle (GOx-AuNP-mAb_2) are employed as immunosensing probe and signal probe, respectively. The H_2O_2 as an excellent holes scavenger that in suit generated from GOx oxidization glucose substrate significantly amplifies the photocurrent. The variation of instantaneous current value that registered as the signal of the immunoassay increases linearly with the logarithm of target PSA concentration increasing in a wide range from 10 pg mL^{-1} to 100 ng mL^{-1} with a low detection limit (LOD) of 4.0 pg mL^{-1}. The SP-PEC immunosensing platform not only simplifies the assay process, but also improves detecting efficiency. The semiautomatic and portable SP-PEC analysis device allows analysis on spot and high-throughput continuous detection. Additional, we also gain deep insight into the relations between the specific shape as well as Au nanocrystal decoration and PEC activity and speculate the possible enhancement mechanisms of Au-$BiVO_4$. Therefore, the present work not only develops a flexible SP-PEC biosensor platform for rapid and continuous detection, but also provides a possible route for designing high performance photoelectric materials.

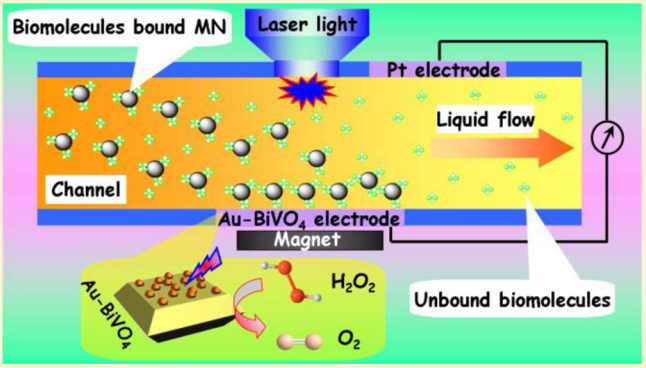

With the growing demands of biomedicine and accurate therapy, improving detection sensitivity, tailing detection time and simplifying procedures are the development trend.[1−4] High sensitivity and accuracy detection prognostic indicator of tumor in early stage cancer is particularly significant because early diagnosis provides the best opportunity for effective treatment.[5,6] The key to the detection is the selective recognition as well as sensitive response to targets.[7] Conventional methods for immunoassay include enzyme-linked immunosorbent assay (ELISA), chemiluminescence, fluorescence, electrochemical methods, mass spectrometry, and Raman spectrometry. However, these methods often suffer from some of drawbacks such as the need of expensive or bulky equipment, tedious procedure, long analysis time, unsatisfactory detectable limitation, and sensitivity. Benefiting from separated trigger signal and detection signal, the PEC bioanalysis exhibits lower background and higher sensitivity comparing with traditional electrochemical and optical methods and has been recognized as a promising methodology for disease diagnosis.[8] Many researchers have been putting sustained efforts to perfect PEC detection methods and expect these methods to serve a wider field. Ju's group constructed a wavelength-resolved ratiometric photoelectrochemical (WR-PEC) sensor with good sensitivity and anti-interference ability for trace analysis in complex samples.[9] Kun et al. designed CdS/RGO/ZnO heterostructure to construct a self-powered PEC biosensor for

Received: November 13, 2016
Accepted: November 23, 2016
Published: November 23, 2016

DOI: 10.1021/acs.analchem.6b04461
Anal. Chem. XXXX, XXX, XXX−XXX

Scheme 1. Schematic Illustration of the (A) Semi-Automated Support Power-Free Photoelectrochemical (SP-PEC) Immunosensing Platform Coupling with a Miniature Semiautomatic Microfluidic System and DMM Readout; (B) Measurement Principle of SP-PEC Immunoassay for PSA

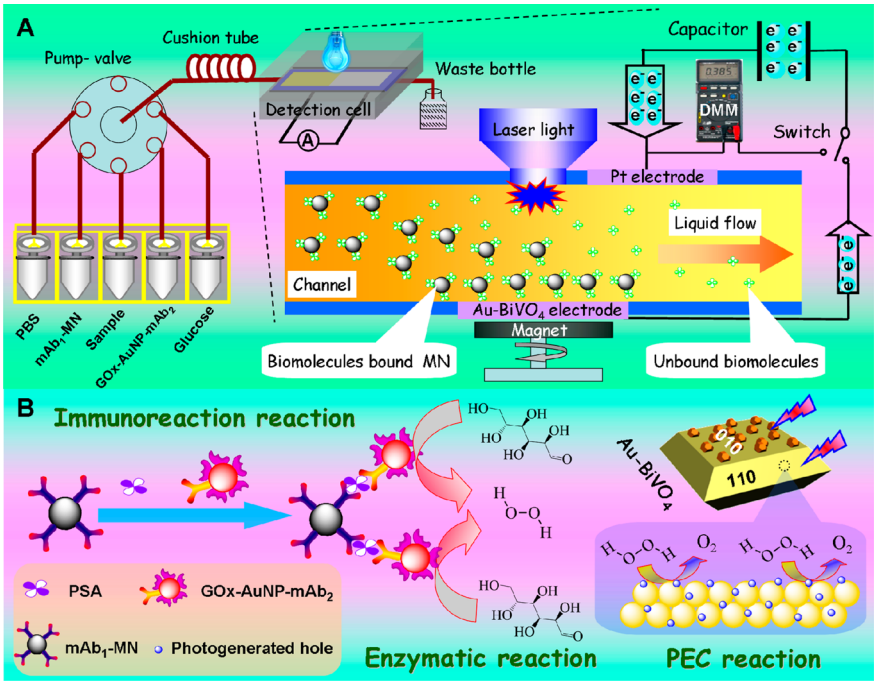

glutathione detection.[10] Willner's group introduced a PEC biosensor without external irradiation for probing enzyme activities and DNA sensing by chemiluminescence resonance energy transfer.[11] To date, despite the novel PEC detection strategies expand rapidly in recent years, commercial applications of PEC biosensor is rare because it still faces some problems and is challenged in routine operating requirements. One important issue of PEC methods lies in the design of determination modes and devices.[12] The traditional PEC biosensors involve the demand of miscellaneous devices, such as the external exciting light source, monochromator, computer and electrochemical workstation, dark box, and so on. These PEC determination modes are unsuitable for routine use and hardly develop into a user-friendly and low-cost assay protocol. The biomolecules, used as biorecognition elements, are fixed onto the sensing surface based photoelectric materials via physical or chemical bonding in the conventional PEC immunoassays. The poor biocompatibility shows by most photoelectric materials may decrease the biological activity of biomolecules. In addition, biological recognition process (e.g., antigen−antibody reaction) and signal monitoring are carried out on the same modified electrode in the most PEC biosensors currently. The PEC biosensors are usually inefficient and even suffer from disposable use because the analyte attaches to the sensing interface and cannot be removed quickly and effectively after finish detection.[13] Even if the complicated manufacturing process and use-cost are ignored, the analytical efficiency and the reproducibility still limited for large quantity complex samples analysis. All of these constrained the advancement and application of the current systems. So, the new sensing modes and devices for high-efficiency and sensitive immunoassay are still needed.

In previous work, our group proposed a new split-type PEC immunosensing strategy to address a series imperfection of conventional PEC immunoassays that result from immobilizing biomolecules onto the photoelectric material.[14] However, it was not a sufficiently ideal approach. The two-step assay format was performed and the product of the enzymatic oxidate was artificially injected into the PEC detection cell. This is a time-consuming and tedious procedure and would be error prone by manual operation because hands-on operations often become main error source of an assay in the test protocol.[15] On the other hand, the local concentration of the enzymatic oxidate, which is used as coreagent to amplify the photocurrent, was diluted during the transfer process, which decreases the PEC immunoassay sensitivity. Last but not least, in order to satisfy the demands of high-throughput analysis, the PEC analytical devices should be improved. Nowadays, one of the great challenges, and also an ongoing effort, is to develop simple, highly sensitive, and yet high-throughput and automatic technologies for biomedical analysis, especially rapid detection of disease-specific biomarkers on the spot.[16] Therefore, constructing an automatic or semiautomatic PEC immunosensing platform for portable and high-throughput continuous monitoring is highly desirable.

Simultaneously, since PEC biosensing monitor the electrical signal change of a electrode and the photon-to-charge conversion process completed in the photoelectric materials, the performance of PEC biosensors significantly rely on composed of sensing interface.[17] The photoelectric materials of a successful PEC biosensor should be highly sensitive to the surface microenvironment fluctuation. Therefore, efficient separating and fast transferring photogenerated charge carriers is the key step in achieving high PEC performance. Recently, monoclinic bismuth vanadate ($BiVO_4$) with small band gap (~2.4 eV) has been considered as a substantially attractive candidate for constructing the PEC sensor due to the advantages such as nontoxicity, long-term chemical stability and low cost.[18] According to the fact that enhanced

DOI: 10.1021/acs.analchem.6b04461
Anal. Chem. XXXX, XXX, XXX−XXX

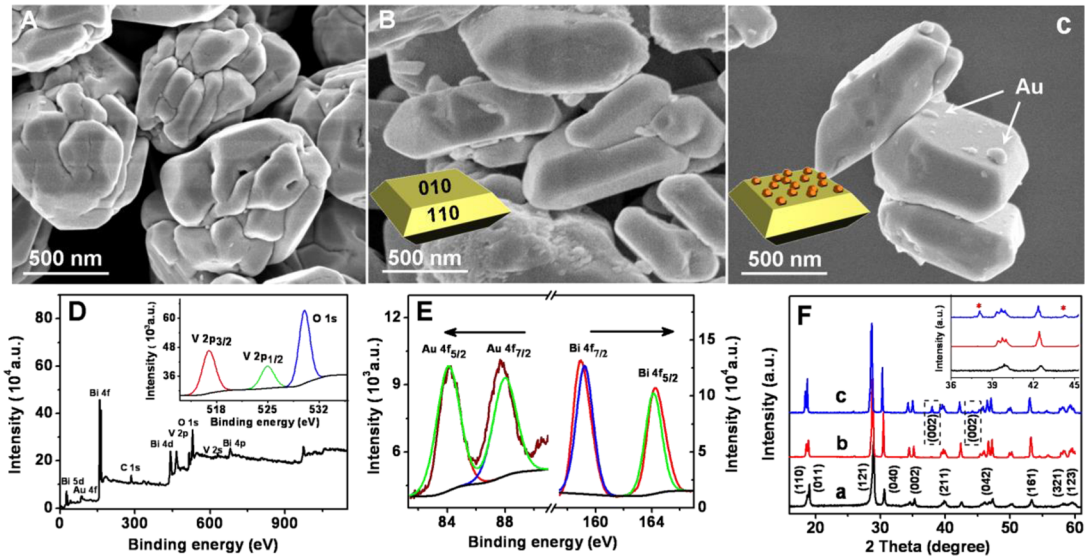

Figure 1. Typical SEM images of (A) I-$BiVO_4$, (B) D-$BiVO_4$, and (C) Au-$BiVO_4$; (D) the overall XPS spectrum of Au-$BiVO_4$ (inset: high-resolution XPS spectra of V and O elements) and (E) high-resolution XPS spectra of Bi and Au elements; (F) XRD and HRXRD (inset) patterns of (a) I-$BiVO_4$, (b) D-$BiVO_4$, and (c) Au-$BiVO_4$.

photocatalytic activity has been achieved from $BiVO_4$ with various well-defined morphologies such as one-dimensional nanorods and nanotubes, two-dimensional nanosheets, and three-dimensional hollow spheres, the morphology and microstructure play crucial roles in the $BiVO_4$ properties.[19] The higher specific surface area, better crystallization and fewer structural defects are beneficial for improving the PEC efficiency. However, the PEC efficiency of pristine $BiVO_4$ is still not impressive because it suffers from recombination of bulk charge carriers and poor electrons transfer property, especially in irregular shape and big crystal size $BiVO_4$.[20] To date, substantial interest and investigation have been focused on incorporating functional micronano materials to construct sensing interface. On the basis of various reports of noble metals modulating the photocatalysis and the energy-level structure of $BiVO_4$, decorating Au nanocrystal onto $BiVO_4$ surface seems to be a feasible strategy to regulate the PEC efficiencies.[21−23]

In a coherent context, herein, an innovative and portable semiautomated support power-free photoelectrochemical immunosensing platform (SP-PEC) with digital multimeter (DMM) readout coupling with a miniature semiautomated injection system and a flow-through detection cell attached a micro blue laser (5w, $\lambda \geq 380$ nm) was designed for flexible detection prognostic indicator of tumor. The nanocomposite that $BiVO_4$ showing decahedral shape with Au nanocrystal selectively demonstrated on the high-active {010} facets (Au-$BiVO_4$) was used as photoanode to achieve optoelectronic converting and exhibited significantly enhanced PEC performance such as satisfactory stability, lowest charge transfer resistance, and high photocurrent intensity under visible light irradiation. We also tried to gain insight into the mechanism behind these effects. This work combined the sensitivity of PEC measurement with convenience of semiautomatic sampling as well as high separation efficiency of magnetic beads, which provided higher precision, stability and determination speed over manual procedures of conventional PEC detections. Therefore, the flexible SP-PEC biosensing platform has opened up a promising channel for the development of novel PEC biosensors for rapid and high-throughput on site diagnosis.

EXPERIMENTAL SECTION

SP-PEC Immunoassay for PSA. The schematic of SP-PEC analysis device and the SP-PEC immunoassay for target PSA based on in situ generation of hole scavenger (H_2O_2) to assist signal amplification strategy are depicted in Scheme 1. The whole device is composed of a miniature semiautomatic injection system, flow-through detection channel attached a micro blue laser light (5w, $\lambda \geq 380$ nm) and digital multimeter (DMM) readout coupling with capacitor. A six port rotary valve equipped with a syringe pump is connected with vial and flow-through detection cell through polytetrafluoroethylene tubes in the miniature semiautomatic injection system. The flow direction was controlled by valve and the flow rate was controlled at 800 μL min^{-1} by syringe pump. The Pt foil and Au-$BiVO_4$ modified special indium doped tin oxide electrode (ITO) was installed in the detection channel of detection cell and connected with external circuit. Partial experimental sections such as preparation of mAb_1-MN immunosensing probe and GOx-AuNP-mAb_2 signal probe were described in the Supporting Information. The one-step sandwich immunoassay process was briefly described as follows: (i) 100 μL of mAb_1-MN (~10 mg mL^{-1}) was injected into the cell and collected near the electrode surface by an external magnet; (ii) 100 μL of PSA standard or sample with various concentrations was injected into the cell followed by 100 μL of the GOx-AuNP-mAb_2 injected to form the sandwich immunocomplex without the magnet. After 35 min, 500 μL of PBS washing solution was flowed through the cell continuously to wash unbinding biomolecules in the presence of magnet and then 200 μL of PBS containing glucose substrate (2 mM) was injected subsequently and reacted for 14 min in the absence of magnet. The in situ generated H_2O_2 scavenged the hole and accelerated the PEC reaction of Au-$BiVO_4$ photoanode under blue light irradiation. The produced charges between two electrodes were collected by capacitor with the switch turned to Au-$BiVO_4$ photoanode (for 30 s). Turning switch from the photoanode to

DOI: 10.1021/acs.analchem.6b04461
Anal. Chem. XXXX, XXX, XXX−XXX

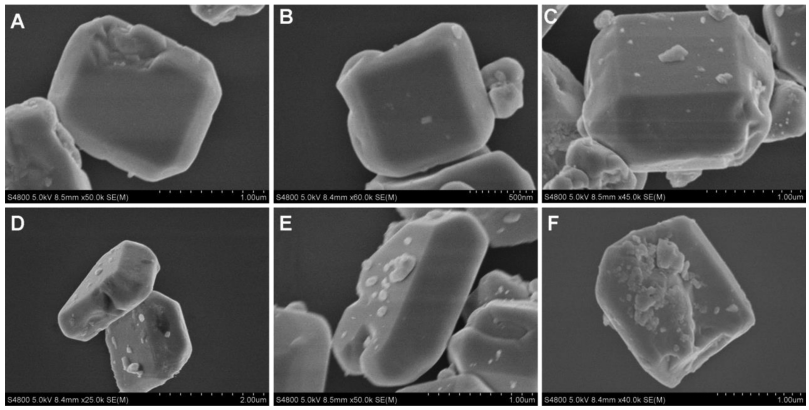

Figure 2. Typical SEM images of Au-$BiVO_4$ with various Au content: (A) 0, (B) 0.2, (C) 0.5, (D) 1, (E) 2, and (F) 5 wt %.

DMM, the capacitor discharged the collected charges to produce an instantaneous current. The variation of instantaneous current value recorded by a nimble DMM registered as the sensor signal to intuitively monitor the PSA concentration. When a detection process was completed, PBS washing solution was injected subsequently by syringe pump to rinse the flow-through detection cell in the absence of external magnet and ready for next samples PEC measurement.

RESULTS AND DISCUSSION

Characterization and PEC Performance of the Nanocomposites. The whole analysis device and detection pathway of the SP-PEC immunoassay platform toward target PSA depicts in Scheme 1. Since the photocurrent response generated from Au-$BiVO_4$ photoanode, the successful preparation of Au-$BiVO_4$ nanocomposite was crucial to the performance of PEC immunoassay. In order to explore and highlight the effects of $BiVO_4$ morphology and Au nanocrystal deposition on PEC activity, irregular shape $BiVO_4$ (I-$BiVO_4$) and decahedral $BiVO_4$ without Au nanocrystal (D-$BiVO_4$) were also prepared and the detail preparation process described in the Supporting Information. It was easily observed that the color of $BiVO_4$ suspension varied from yellow to light green after deposited Au nanocrystal (Figure S-1). The morphologies intuitively revealed by scanning electron microscopy (SEM). The I-$BiVO_4$ (Figure 1A) formed by stacking various small particles and lacked specific shape and size while D-$BiVO_4$ (Figure 1B) exhibited defined decahedral shape that consisted with top and bottom flat surfaces ({010} facets) and isosceles trapezoidal sides ({110} facets). The size of D-$BiVO_4$ distributed from about 0.5 to 1.5 um and thickness was about 300 nm. Different from smooth facets exposed in D-$BiVO_4$, many white dots of photodeposited Au nanocrystal could be observed on {010} facets in Au-$BiVO_4$ composites (Figure 1C). Meanwhile, a tiny amount of Au nanocrystal deposited on the {110} facets, which was consistent with the fact that pure $BiVO_4$ cannot achieve electron−hole separation completely on the {010} and {110} facets.[24] Subsequently, the chemical component and elements chemical state of Au-$BiVO_4$ composites was confirmed by X-ray photoelectron spectroscopy (XPS). The characteristic peaks of Bi, V, and O and Au could be observed as expected in the overall XPS spectrum (Figure 1D). The peaks appeared in high-resolution XPS spectrum located at 516, 524, and 530.1 eV corresponded to V $2p_{1/2}$, V $2p_{3/2}$, and O 1s bands (inset in Figure 1D), respectively. The binding energies of 158.9 and 164.1 eV assigned to Bi $4f_{7/2}$ and Bi $4f_{5/2}$ of Bi^{3+} in $BiVO_4$, respectively (Figure 1E). Notably, peaks with binding energies of 84.2 and 89 eV corresponding to Au $4f_{7/2}$ and Au $4f_{5/2}$ of Au nanocrystal corroborated that $HAuCl_4$ was reduced to metallic gold.[25] Additionally, I-$BiVO_4$, D-$BiVO_4$ and Au-$BiVO_4$ prepared with different method and process, whether the crystal phase transition or structure change need to be answered. Here, X-ray diffraction (XRD) was employed to investigate the all samples. The diffraction peaks of all samples (Figure 1F) corresponded to the JCPD card number 14−0688, which identified samples were crystalline and presented single monoclinic scheelite structure. Single monoclinic structure is the thermodynamically stable phase, and exhibits excellent PEC activity for $BiVO_4$. D-$BiVO_4$ and Au-$BiVO_4$ exhibited the sharper diffraction peaks and higher intensity comparing with I-BiVO4, which indicated the D-$BiVO_4$ and Au-$BiVO_4$ had higher crystallinity and purer phase. Additionally, the distinct diffraction peaks at 38.0° and 44.2° that only appeared in Au-$BiVO_4$ could be assigned to the (111) and (200) plane of Au nanocrystal (JCPDS No. 01−089−3697), respectively.[26] This result powerful validated Au nanocrystal successful deposition on D-$BiVO_4$ and crystal structures of D-$BiVO_4$ changed almost nothing after photodepositon of Au nanocrystal. The results of SEM, XPS and XRD both demonstrated that no significant changes in terms of $BiVO_4$ original morphologies, size distribution and crystal structures and Au element merely existed with metallic Au on the surface of D-$BiVO_4$ and did not dope into the crystal lattice.

The successful preparation of Au-$BiVO_4$ allowed us to investigate one of the great concerns that whether the PEC activity could be significantly enhanced by adjusting the morphology and photodepositing Au nanocrystal. At the same time, the content of Au on surface of D-$BiVO_4$ was optimized from 0, 0.2, 0.5, 1, 2, and 5 wt %. The micrographs indicated that the higher initial $HAuCl_4$ content tended to grow denser and bigger Au nanocrystal on the {010} facets of Au-$BiVO_4$ (Figure 2). Here, the PEC activity of samples were examined in terms of the photocatalytic reaction rate by using methylene blue (MB) dye as the probe molecule in aqueous solution with visible light irradiation ($\lambda > 420$ nm).[27] The rate constant calculated from Langmuir−Hinshelwood kinetic: $\ln(C_0/C) = kt + a$, where C_0, C, and k are the initial and real time concentration of dye and apparent reaction rate constant, respectively.[28] As might be expected, D-$BiVO_4$ exhibited slightly higher photocatalytic activities than I-$BiVO_4$. The content of Au had a significantly influence to the photocatalytic

DOI: 10.1021/acs.analchem.6b04461
Anal. Chem. XXXX, XXX, XXX−XXX

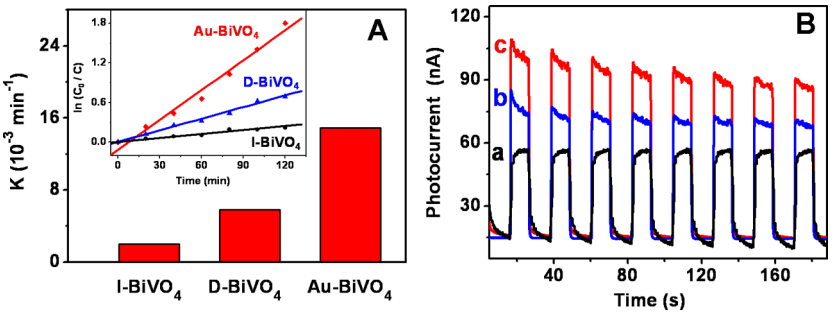

Figure 3. (A) Reaction rate constants (k) of samples on photocatalytic degradation of MB (inset: the linear fitting pseudo-first-order MB decay curves); (B) transient photocurrent responses of (a) I-$BiVO_4$, (b) D-$BiVO_4$, and (c) 2 wt % Au-$BiVO_4$ (recorded and irradiated by three electrodes system and 300 W xenon lamp, respectively).

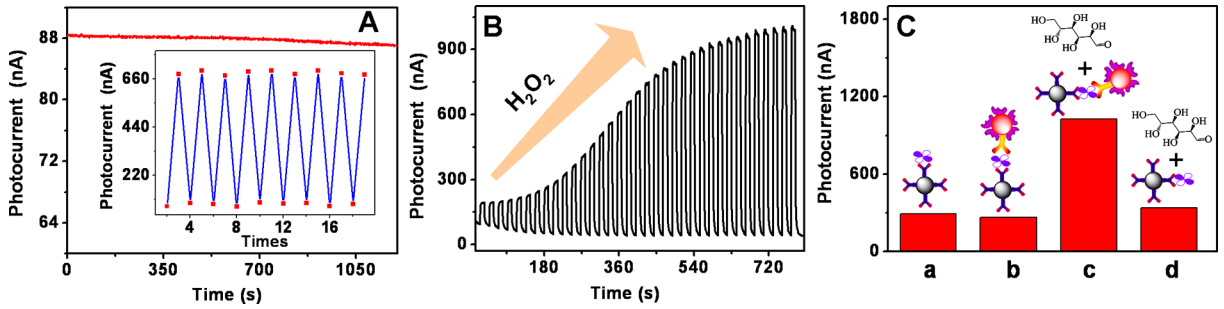

Figure 4. Photocurrent of (A) the Au-$BiVO_4$/ITO measured at 0 V under continuous illumination (inset: the photocurrent of alternate injection of PBS buffer and H_2O_2 solution) and (B) sequential introduction gradient concentration H_2O_2 under repeated on and off cycles of illumination; (C) the photocurrent of control tests: (a) mAb_1-MN + PSA, (b) mAb_1-MN + PSA + GOx-AuNP-mAb_2, (c) mAb_1-MN + PSA + GOx-AuNP-mAb_2 + glucose, and (d) mAb_1-MN + PSA + glucose, respectively.

activity and the Au-$BiVO_4$ prepared by 2 wt % $HAuCl_4$ exhibited highest activity in all these samples, thus, this content was chosen for the next discussion. The reaction rate constants of I-$BiVO_4$, D-$BiVO_4$, and 2 wt % D-$BiVO_4$ were shown in Figure 3A. The absorption spectra of photocatalytic degradation of MB by 2 wt % Au-$BiVO_4$ was shown in Figure S-2. Furthermore, the transient photocurrent response was examined by electrochemical workstation with a standard three-electrode system in PBS electrolyte at 0 V (vs SCE). Comparing the photocurrent temporal curve, Au-$BiVO_4$ showed highest photocurrent intensity and followed by D-$BiVO_4$ (Figure 3B), which paralleled the photocatalytic activity result. These results indicated that the regular decahedral morphology with exposed {010} facet could improve photoactivity to a certain extent and subsequent deposition of Au nanocrystal on D-$BiVO_4$ could significant improve PEC performance.

Many researches have shown that semiconductor-based nanocomposites modified with noble metals exhibit great promise for applications in sensor, environmental remediation, optoelectronics, energy conversion, and other areas. However, the specific behavior of noble metal on these processes is still ambiguous and without a uniform conclusion so far.[29,30] Understanding the mechanism of decahedral morphology and Au nanocrystal improving PEC activity is another great concerns and fascinating question because it is beneficial for us to build better applications and services. The detailed experimental process and discussion about the PEC enhancement mechanisms were presented in Supporting Information. The mechanisms summarize briefly as follows: first, the energy levels differences of D-$BiVO_4$ between the {010} and {110} facets of valence band (VB) and conduction band (CB) force the most electrons and holes migrate to different facets and inhibit the charger carriers recombination in the bulk; then Au nanocrystal worked as a conducting scaffold quickly transferring accumulated electrons in the {010} facet and suppress recombination on D-$BiVO_4$ surface. Under the synergistic action of morphology to the bulk charge separation and Au nanocrystal to the surface charge transfer, the electron−hole recombination is suppressed significantly.

Feasibility of the SP-PEC Immunoassay Platform. On the basis of the efficient separation of charge carriers in the bulk and fast electrons transfer in the surface of Au-$BiVO_4$, it is reasonable for us to speculate the PEC biosensor that employing Au-$BiVO_4$ as a photoanode could exhibit excellent performance. The device, detection principle, and process of SP-PEC immunoassay for PSA were illustrated in Scheme 1. In the proposed SP-PEC immunoassay PSA, monoclonal anti-PSA capture antibody (mAb_1)-functionalized Fe_3O_4 magnetic nanobeads (mAb_1-MN) and glucose oxidase and detection antibody-conjugated gold nanoparticles (GOx-AuNP-mAb_2) were used as model analyte, immunosensing probe, and signal probe, respectively. The sandwich immunocomplex was formed in the detection channel after the composite successively injected into the cell by syringe pump in the presence of external magnet. Glucose substrate can be catalyzed by the GOx to produce H_2O_2. Irradiation of laser light could induce Au-$BiVO_4$ photoanode to produce a voltage to charge the external capacitor. Here, the in situ generated H_2O_2 was chosen to significantly amplify the signal by scavenging the photogenerated holes at the surface of Au-$BiVO_4$ photoanode because it is transparent to light and has an oxidation rate 1−2 orders of magnitude higher than that of H_2O. More important, comparing with the reduction potential of H_2O (E^{θ}

DOI: 10.1021/acs.analchem.6b04461
Anal. Chem. XXXX, XXX, XXX−XXX

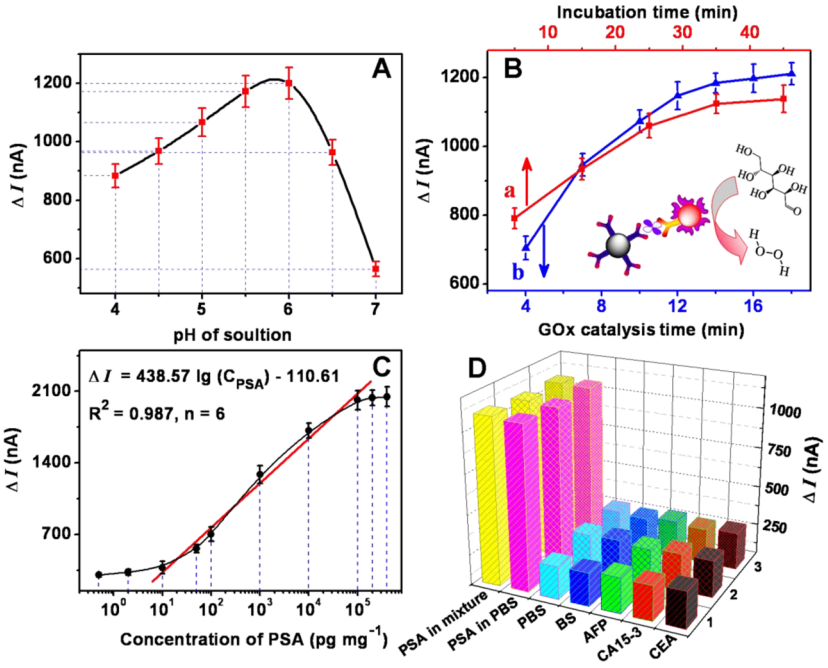

Figure 5. Influence of (A) pH of PBS solution and time (B) for (a) GOx catalytic glucose and (b) incubation on the photocurrent of the SP-PEC immunoassay; (C) calibration plots of ΔI vs logarithm of the PSA standards concentrations and (D) the assessment of selectivity and specificity of the proposed PEC immunoassay to the interfering substances: CEA (10 ng mL^{-1}), CA15−3 (10 ng mL^{-1}), AFP (10 ng mL^{-1}), bovine serum (BS), and their mixture.

= +1.23V_{RHE}), H_2O_2 has a relatively negative potential (E^{θ} = +0.68V_{RHE}). Since the SP-PEC device was designed for high-throughput continuous detecting, the toleration of light irradiation and rapid response to H_2O_2 was essential. As shown in Figure 4A, the photocurrent was highly stable under continuous light radiation. The relative standard deviation (RSD) of photocurrent response to PBS buffer (6.8%) and H_2O_2 (2.3%) was acceptable with the PBS and H_2O_2 solution alternately injected (Figure 4A, inset). Furthermore, to visually reflect the sensitive response to H_2O_2 concentration change and potential to continuous detection, a series concentration of H_2O_2 was sequentially injected into the SP-PEC device that connected with an electrochemical workstation. With the increasing of H_2O_2 concentration in the solution, photocurrent intensity increased rapidly and significantly (Figure 4B) at 0 V. The more H_2O_2 the solution contained, the higher photocurrent it achieved. Thus, the SP-PEC analysis device constructed by Au-$BiVO_4$ photoanode could be employed for continuous target monitoring. Comparing with modified electrodes of traditional PEC biosensor, the Au-$BiVO_4$ photoanode behaved like a photovoltaic cell as it stably generated photocurrent without other external electrical power input under visible light irradiation.[31] Thus, the advantage of Au-$BiVO_4$ exhibited in low potential is in line with our design for PEC biosensor application.

Finally, to confirm the feasibility of immunoassay for PSA and whether the PEC reaction could be smoothly progressed in the presence of GOx and glucose, several control tests were implemented (Figure 4C). The enhanced photocurrent (the data obtained by DMM) was only achieved when mAb_1-MN, PSA (0.5 ng mL^{-1}), GOx-AuNP-mAb_2, and glucose substrate existed simultaneously. Additionally, the glucose substrate showed little influence to the photocurrent. This result indicated that the enhanced signal originated from enzymatic oxidate (H_2O_2) scavenged the hole in the presence of target PSA. Obviously, highly specific sandwich immunoreaction among mAb_1-MN, PSA, and GOx-AuNP-pAb_2 and highly efficient catalysis of GOx to glucose were the bulwark of immunoassay for PSA. In a certain concentration range, the more PSA existed, the higher photocurrent generated. Thus, the current signal variation depended significantly on the concentration of PSA.

Analytical Performance of SP-PEC for PSA Detection. The excellent PEC activity of Au-$BiVO_4$, specific sandwich immunoreaction and highly efficient catalysis are vital to the proposed immunoassay. For the sake of the optimal analytical performance, pH of solution, incubation time for antigen−antibody reaction and catalytic time of GOx toward to glucose were optimized separately (0.5 ng mL^{-1} PSA used in the all cases). Figure 5A depicted the dependence of the photocurrent on the pH of solution. The slow but steady increase of variations of photocurrent ($\Delta I = I_{target} - I_{background}$, where I_{target} and $I_{background}$ are the instantaneous current in the presence and absence of target) was observed with the pH value rise in the range from 4.0 to 6.0. However, the photocurrent decreased sharply with the pH further increase. This phenomenon can be explained by the fact that weak acidic environment is beneficial for H_2O_2 generation by improving the catalytic activity of GOx and excessively high or low pH solution leads to GOx inactivation. So, the pH 6.0 of PBS was used in whole detection. As shown in Figure 5B, the ΔI raised with the extending time and gradually reached to a plateau at 35 and 14 min for incubation (curve *a*) and catalysis (curve *b*), respectively. Considering the minimizing detection time and maximizing efficiency of the assay, 35 and 14 min was chosen for incubation and catalysis, respectively.

Under the optimum conditions, quantitative analysis of the proposed SP-PEC immunosensing platform for PSA in standard solution was performed. The ΔI that obtained by DMM linearly increased with the logarithm of PSA

DOI: 10.1021/acs.analchem.6b04461
Anal. Chem. XXXX, XXX, XXX−XXX

Table 1. Comparison of SP-PEC Immunoassay with Commercial PSA ELISA Kit for Human Serum Samples

	method accuracy; conc. (mean ± SD, ng mL^{-1}, n = 3);[b] t-test			recovery evaluation[d]		
sample No.[a]	PEC immunoassay	PSA ELISA kit	t_{exp}	added (ng mL^{-1})[c]	found (ng mL^{-1})	recovery (%)
1	5.56 ± 0.47	6.21 ± 0.35	1.92	1.0	6.73 ± 0.44	117
2	0.28 ± 0.02	0.31 ± 0.01	2.33	0.1	0.39 ± 0.36	110
3	19.21 ± 1.72	17.97 ± 1.59	0.92	15.0	33.36 ± 2.73	94.3
4	0.08 ± 0.007	0.1 ± 0.006	1.88	1.0	1.07 ± 0.98	99
5	21.82 ± 1.77	20.46 ± 1.35	1.06	20.0	41.06 ± 3.94	96.2
6	14.7 ± 1.54	15.9 ± 1.43	0.99	10	25.65 ± 2.02	110
7	0.59 ± 0.03	0.65 ± 0.04	2.10	0.5	1.11 ± 0.09	104
8	3.39 ± 0.27	3.13 ± 0.22	1.29	5.0	8.62 ± 0.82	104.6

[a]Sample Nos. 1−5 were detected directly and sample Nos. 6−8 were detected by diluting sample No. 5 to different concentrations with PBS. [b]The contents of PSA in these samples were measured by PEC immunoassay and PSA ELISA kit according to the respective calibration curve. [c]PSA standards with different concentrations were added into the initial human serum samples, respectively. [d]The data was obtained according to PEC immunoassay and the recovery was calculated as the following equation: $(C_{found} - C_{sample}) \div C_{added} \times 100\%$. All data as mean ± SD were obtained on the basis of three measurements.

concentration increasing over a range of 10 pg mL^{-1} to 100 ng mL^{-1} (Figure 5C). The linear equation for derived calibration curve was ΔI (nA) = 438.57 × lg C[$_{PSA}$] − 110.61 (pg mL^{-1}, R^2 = 0.987, n = 5) and the detection limit (LOD) was about 4 pg/mL^{-1} (estimated from the expression of $3S/K$, where S is the standard deviation for 11 determinations of blank solution and K is the slope of the calibration plot). The LOD achieved by this strategy was significantly below the clinical cutoff value for the diagnosis of prostate cancer. The all data points were the average value of five parallel detections, and the maximum relative standard deviations (RSD) of data points were below 8.6%, which suggested a high reproducibility and precision of the SP-PEC immunosensing platform. Finally, some possible biomarkers coexisting in human serum and complicated matrix proteins were employed to evaluate the selectivity and specificity of SP-PEC immunosensing platform because these characteristics were extremely important for the practical applications.[15] As shown in Figure 5D, the responses to the interfering agents and bovine serum (BS) were close to that of the blank sample (PBS). The responses to the mixture that containing target PSA was similar to that of the PSA standard solution. These observations robustly supported that the SP-PEC immunosensing platform possessed excellent selectivity and anti-interference ability.

On the basis of the above results, the SP-PEC immunoassay challenged to monitor the PSA in human serum samples that were collected from a local hospital for evaluating the potential in clinical applications. The concentrations of PSA detected by the SP-PEC immunoassay were calculated according to the calibration curve depicted in Figure 5C. Statistical comparison between the experimental results of SP-PEC immunoassay and commercial human PSA-total ELISA kit (Sigma, linear range: 0.1−50 ng mL^{-1} and LOD: 0.06 ng mL^{-1}) were carried out with an unpaired Student's t test, preceded by the application of an F-test. The statistics for each sample was calculated by using an independent two-sample t test with equal sample sizes and equal variance as follows:

$$t = \frac{|\bar{x}_1 - \bar{x}_2|}{s_{x1x2}} \sqrt{\frac{n}{2}} \quad (1)$$

where

$$s_{x1x2} = \sqrt{\frac{s_{x1}^2 + s_{x2}^2}{2}} \quad (2)$$

The $\bar{x}$, S_x, and n represent the mean, standard deviation, and times of parallel detection of the sample (1 means the data obtained from the proposed method and 2 means the data obtained from reference method), respectively. The results of these two methods are listed in Table 1 as mean ± SD and the all t_{exp} are lower than t_{crit} (t_{crit}[0.05,4] = 2.78). The mean concentrations of PSA in serum detected by SP-PEC immunoassay and reference method had no significant difference at the confidence level of 95%. Furthermore, recovery experiment was also employed to evaluate the applicability of the SP-PEC immunoassay by the standard addition method. The all recovery values in the range of 94 to 117% were satisfying. These results consistently indicated that the SP-PEC immunoassay had a satisfactory performance for detection of PSA in real samples and could be used as an alternative method for PSA assay. It is also worth noting that the antigen−antibody was used as a biorecognition element for selectively monitoring the desired target. Employing the different biorecognition elements, the methodology could be utilized to precisely analyze a wider range of biological ingredients. Thus, it represented a flexible and versatile PEC detection protocol.

CONCLUSIONS

In summary, this work reports an innovative and power-free photoelectrochemical immunosensing platform consisting of a semiautomatic flow-through device and a portable digital multimeter for disease-related biomarkers (PSA used in this case). The decahedral Au-$BiVO_4$ nanocomposite with Au nanocrystal selectively decorated on the high-active {010} facets was used as the photoanode materials. Results revealed that crystal facet modification had a great effect on surface charge population of photoelectric materials under visible light irradiation. The SP-PEC immunosensing system could effectively overwhelm serious drawbacks of traditional PEC immunosensors as follows: (i) Introduction of magnetic controlled immunosensing system not only remained the in situ generation of hole scavenger to amplify the photocurrents, but effectively simplified the fabrication of the sensing interface and its reuse; (ii) Use of miniature semiautomatic microfluidic device enhanced the detection efficiency; and (iii) Utilization of the digital multimeter provided a portable and low-cost transducer for signal readout relative to classical electrochemical workstation. Nevertheless, one defect of this work depended on the automation and integration improvement of

DOI: 10.1021/acs.analchem.6b04461
Anal. Chem. XXXX, XXX, XXX−XXX

the whole device for intelligent flexible analysis in the future. To the best of our knowledge, this was the first work focusing on a magnetically controlled microfluidic device for the development of a simple and portable PCE immunoassay.

■ ASSOCIATED CONTENT

Supporting Information

The Supporting Information is available free of charge on the ACS Publications website at DOI: 10.1021/acs.analchem.6b04461.

Experimental section, photographs of D-$BiVO_4$ and Au-$BiVO_4$ (Figure S-1), photocatalytic degradation MB by 2 wt % Au-$BiVO_4$ (Figure S-2), and the study about Au-$BiVO_4$ PEC activity enhancement mechanisms (PDF).

■ AUTHOR INFORMATION

Corresponding Author

*Phone: +86-591-2286 6125. Fax: +86-591-2286 6135. E-mail: dianping.tang@fzu.edu.cn.

ORCID

Dianping Tang: 0000-0002-0134-3983

Notes

The authors declare no competing financial interest.

■ ACKNOWLEDGMENTS

This work was financially supported by the National Natural Science Foundation of China (Grant Nos.: 21675029 and 21475025), the National Science Foundation of Fujian Province (Grant No.: 2014J07001), and the Program for Changjiang Scholars and Innovative Research Team in University (Grant No.: IRT15R11).

■ REFERENCES

(1) Chen, G.; Roy, I.; Yang, C.; Prasad, P. N. *Chem. Rev.* **2016**, *116*, 2826−2885.
(2) Wang, Y.; Vaidyanathan, R.; Shiddiky, M J. A.; Trau, M. *ACS Nano* **2015**, *9*, 6354−6362.
(3) Wu, C.; Han, D.; Chen, T.; Peng, L.; Zhu, G.; You, M.; Qiu, L.; Sefah, K.; Zhang, X.; Tan, W. *J. Am. Chem. Soc.* **2013**, *135*, 18644−18650.
(4) Nguyen, K. T.; Zhao, Y. *Acc. Chem. Res.* **2015**, *48*, 3016−3025.
(5) Wang, H.; Yuan, Y.; Chai, Y.; Yuan, R. *Small* **2015**, *11*, 3703−3709.
(6) Kim, J.; Jang, M.; Lee, K. G.; Lee, K. S.; Lee, S. J.; Ro, K. W.; Kang, I. S.; Jeong, B. D.; Park, T. J.; Kim, H. J.; Lee, J. *ACS Appl. Mater. Interfaces* **2016**, *8*, 23489−23497.
(7) Sun, J.; Hu, T.; Chen, C.; Zhao, D.; Yang, F.; Yang, X. *Anal. Chem.* **2016**, *88*, 9789−9795.
(8) Zhao, W. W.; Xu, J. J.; Chen, H. Y. *Chem. Soc. Rev.* **2015**, *44*, 729−741.
(9) Hao, Q.; Shan, X.; Lei, J.; Zang, Y.; Yang, Q.; Ju, H. *Chem. Sci.* **2016**, *7*, 774−780.
(10) Zhao, K.; Yan, X.; Gu, Y.; Kang, Z.; Bai, Z.; Cao, S.; Liu, Y.; Zhang, X.; Zhang, Y. *Small* **2016**, *12*, 245−251.
(11) Golub, E.; Niazov, A.; Freeman, R.; Zatsepin, M.; Willner, I. *J. Phys. Chem. C* **2012**, *116*, 13827−13834.
(12) Wang, L.; Han, D.; Ni, S.; Ma, W.; Wang, W.; Niu, L. *Chem. Sci.* **2015**, *6*, 6632−6638.
(13) Zhang, C.; Xu, J. Q.; Li, Y. T.; Huang, L.; Pang, D. W.; Ning, Y.; Huang, W. H.; Zhang, Z.; Zhang, G. J. *Anal. Chem.* **2016**, *88*, 4048−4054.
(14) Shu, J.; Qiu, Z.; Zhou, Q.; Lin, Y.; Lu, M.; Tang, D. *Anal. Chem.* **2016**, *88*, 2958−2966.
(15) Huang, Y.; Wang, T. H.; Jiang, J. H.; Shen, G. L.; Yu, R. Q. *Clin. Chem.* **2009**, *55*, 964−971.
(16) Wang, L. J.; Sun, R.; Vasile, T.; Chang, Y. C.; Li, L. *Anal. Chem.* **2016**, *88*, 8302−8308.
(17) Li, C.; Wang, H.; Shen, J.; Tang, B. *Anal. Chem.* **2015**, *87*, 4283−4291.
(18) Li, C.; Wang, S.; Wang, T.; Wei, Y.; Zhang, P.; Gong, J. *Small* **2014**, *10*, 2783−2790.
(19) Park, Y.; McDonald, K. J.; Choi, K. S. *Chem. Soc. Rev.* **2013**, *42*, 2321−2337.
(20) Yehezkeli, O.; Harguindey, A.; Domaille, D. W.; He, L.; Cha, J. N. *RSC Adv.* **2015**, *5*, 58755−58759.
(21) Wang, H.; Zhang, L.; Chen, Z.; Hu, J.; Li, S.; Wang, Z.; Liu, J.; Wang, X. *Chem. Soc. Rev.* **2014**, *43*, 5234−5244.
(22) Bumajdad, A.; Madkour, M. *Phys. Chem. Chem. Phys.* **2014**, *16*, 7146−7158.
(23) Li, R.; Zhang, F.; Wang, D.; Yang, J.; Li, M.; Zhu, J.; Zhou, X.; Han, H.; Li, C. *Nat. Commun.* **2013**, *4*, 1432.
(24) Li, C.; Zhang, P.; Lv, R.; Lu, J.; Wang, T.; Wang, S.; Wang, H.; Gong, J. *Small* **2013**, *9*, 3951−3956.
(25) Zhang, A.; Zhang, J. J. *J. Alloys Compd.* **2010**, *491*, 631−635.
(26) Feng, W.; Wang, B.; Zheng, Z.; Fang, Z.; Wang, Z.; Zhang, S.; Li, Y.; Liu, P. *Appl. Catal., B* **2016**, *186*, 143−150.
(27) Di, J.; Xia, J.; Yin, S.; Xu, H.; Xu, L.; Xu, Y.; He, M.; Li, H. *J. Mater. Chem. A* **2014**, *2*, 5340−5351.
(28) Wu, S.; Zheng, H.; Lian, Y.; Wu, Y. *Mater. Res. Bull.* **2013**, *48*, 2901−2907.
(29) Booshehri, A. Y.; Goh, S. C. K.; Hong, J.; Jiang, R.; Xu, R. *J. Mater. Chem. A* **2014**, *2*, 6209−6217.
(30) Kochuveedu, S. T.; Jang, Y. H.; Kim, D. H. *Chem. Soc. Rev.* **2013**, *42*, 8467−8493.
(31) Zhan, Z.; Zheng, L.; Pan, Y.; Sun, G.; Li, L. *J. Mater. Chem.* **2012**, *22*, 2589−2595.

DOI: 10.1021/acs.analchem.6b04461
Anal. Chem. XXXX, XXX, XXX−XXX